Lab on a Chip

Cite this: *Lab Chip*, 2011, **11**, 4174

www.rsc.org/loc

PAPER

Mass sensors with mechanical traps for weighing single cells in different fluids†

Yaochung Weng,‡[ab] Francisco Feijó Delgado,‡[bc] Sungmin Son,[d] Thomas P. Burg,[e] Steven C. Wasserman[b] and Scott R. Manalis*[bc]

Received 9th August 2011, Accepted 7th October 2011
DOI: 10.1039/c1lc20736a

We present two methods by which single cells can be mechanically trapped and continuously monitored within the suspended microchannel resonator (SMR) mass sensor. Since the fluid surrounding the trapped cell can be quickly and completely replaced on demand, our methods are well suited for measuring changes in cell size and growth in response to drugs or other chemical stimuli. We validate our methods by measuring the density of single polystyrene beads and *Saccharomyces cerevisiae* yeast cells with a precision of approximately 10^{-3} g cm^{-3}, and by monitoring the growth of single mouse lymphoblast cells before and after drug treatment.

1 Introduction

The suspended microchannel resonator (SMR) enables single-cell measurements of buoyant mass with femtogram-level resolution.[1,2] The SMR consists of an embedded microfluidic channel inside a cantilever that resonates in an on-chip vacuum. Cells or particles with a different density than the surrounding fluid cause a small change in the cantilever's resonant frequency as they flow through the cantilever, and their buoyant mass can be determined from the magnitude of the frequency change. The buoyant mass, or mass of a particle in fluid, is defined as

$$m_{buoyant} = V(\rho_p - \rho_f) \quad (1)$$

where V is the particle volume, and ρ_p and ρ_f are the particle and fluid densities, respectively.

Early SMR implementations could provide the buoyant masses of cells in a population but could weigh each cell only once and were unable to monitor single cells over time.[3] Later systems added fluidic controls to implement *dynamic trapping*, during which an individual cell is repeatedly passed back and forth through the SMR. When maintained over extended time periods, this dynamic trap can measure the growth of individual cells in real time.[2] But delivering chemical stimuli to a dynamically trapped cell is challenging because viscous-dominated flow inside the microchannel ensures that the cell moves along with the surrounding fluid.

Recently, Grover, Bryan *et al.* showed that by loading the SMR device with two different fluids, single cells can be dynamically trapped within the two fluids, weighed in the first fluid and then weighed in the second fluid.[4] This technique is well suited for measuring the density of single cells by weighing them in two fluids of different densities. However, their technique is unsuitable for measuring the response of a cell to chemical stimuli because the duration of exposure of the cell to the second fluid is limited to only a few seconds, and the growth rate of a single cell cannot be measured both pre- and post-treatment with a drug. Finally, the buoyant mass measured by this method is subject to uncertainty caused by variations in the cell's flow path through the cantilever.

One strategy for overcoming these limitations is to physically trap each cell within the SMR. The buoyant mass of the cell could then be monitored continuously while the fluid surrounding the cell is changed at will. Several designs for cell traps were considered: methods such as standing acoustic waves,[5] dielectrophoresis[6,7] and optical trapping[8,9] have their appeal in that no cell contact is necessary and that the action of capturing and releasing a cell can be readily controlled. However, while it is possible to generate forces on the order of tens to hundreds of piconewtons by applying acoustic or electromagnetic waves in an ordinary microfluidic channel, the multilayered geometry and complex design of the SMR device make it difficult to implement these techniques. Mechanical structures involving cell-sized 'docks' preceding a constriction[10,11] and U-shaped trapping

[a]*Computational & Systems Biology Initiative, Massachusetts Institute of Technology, Cambridge, MA, 02139, USA*
[b]*Department of Biological Engineering, Massachusetts Institute of Technology, Cambridge, MA, 02139, USA. E-mail: scottm@media.mit.edu*
[c]*Koch Institute for Integrative Cancer Research, Massachusetts Institute of Technology, Cambridge, MA, 02139, USA*
[d]*Department of Mechanical Engineering, Massachusetts Institute of Technology, Cambridge, MA, 02139, USA*
[e]*Max Planck Institute for Biophysical Chemistry, 37077 Göttingen, Germany*

† Electronic supplementary information (ESI) available. See DOI: 10.1039/c1lc20736a

‡ These authors contributed equally to this work.

compartments[12–15] proved to be more robust cell capturers for our application.

Mechanical trapping structures integrated with the SMR can effectively load and unload a single cell while its buoyant mass and the density of the surrounding fluid are continuously monitored. We evaluated two types of mechanical trap: the first, referred to as three-channel SMRs (Fig. 1a,b), proved to be most suitable for single-cell density measurements, while the second type, referred to as columned SMRs (Fig. 1c), was used to measure cell growth before and after exposure to a drug.

2 Three-channel SMRs

2.1 Method

Three-channel SMRs were fabricated as described previously[1] with a capture dock at the apex of the cantilever (Fig. 1a,b) and a third fluidic channel used to control flow into and out of the dock. At the T-junction where the dock meets the third channel (channel 3), a narrow constriction allows fluid to pass, but not cells of the appropriate size. Two versions of the three-channel SMR with different dimensions were fabricated: one with a 3 × 8 μm channel cross-section and a 200 nm wide horizontal slit; and another with an 8 × 8 μm channel cross-section device and a 2 μm wide vertical gap. A computer-controlled fluidic system orchestrates a sequence of pressure changes that traps a cell, measures its buoyant mass, quickly replaces the fluid around the cell, measures its buoyant mass a second time in the new fluid, and ejects the cell.

To prime the device, fluid 1 flows from bypass channel B1 to the cantilever. Fluid 1 carries the cells to be measured (Fig. 2, **blue**). Relative pressure settings ensure that the majority of fluid 1 travels from B1 to the second bypass B2 *via* the SMR to minimize the likelihood of cells being captured in the dock. After the device is primed, the fluid velocity through the SMR is reduced, and pressure on the bypass B3 is lowered so that a significant amount of the fluid now flows through the third channel. Thus, a transiting cell will be directed into the pocket and captured (Fig. 4 **inset**). Cell capture is detected as a stepwise change in the resonant frequency due to the change in mass inside the cantilever (if the cell sinks, mass increases and frequency decreases; if the cell floats, mass decreases and frequency increases). Cell immobilization eliminates position uncertainty, a source of error, which exists when measuring samples in a flow through mode.

After a cell is trapped, the computer reverses the flow to flush the SMR with fluid 2 (Fig. 2, **red**) from bypass channel B2. Fluid 1 is completely rinsed out of the cantilever, leaving the cell immersed in fluid 2. Prior to removing the cell from the trap, bypass B3 is filled with fluid 2, and a constant flow is maintained. This clears out remnants of fluid 1 that have previously exited through the third channel and is crucial for preventing the two fluids from mixing during the ejection step. The control system then gradually pressurizes the third channel until the cell leaves the dock. After the cell is ejected, there is another step in the resonant frequency corresponding to the buoyant mass of the cell in fluid 2. The entire sequence of events takes 3–5 s and can be observed in Supplementary Movie 1, ESI.† The duration of serial measurements depends on cell concentration. Smaller concentrations of cells will increase the delay between measurements, but high concentrations will lead to multiple cells being trapped.

With two buoyant mass measurements and two measurements of the fluid density, the cell's density can be determined. The device is calibrated with fluids of known density, allowing the density of fluids 1 and 2 to be accurately determined. The cell density is, therefore, determined as:

$$\rho_{cell} = \frac{m_{buoyant2} \cdot \rho_{fluid1} - m_{buoyant1} \cdot \rho_{fluid2}}{m_{buoyant2} - m_{buoyant1}} \quad (2)$$

Measurement error in the cell's density is affected by the choice of densities of fluids 1 and 2. If the reference fluid densities are close, the buoyant mass values in both fluids will also be close, and the measurement error will play a more significant role in eqn (2). This error was minimized by choosing reference fluids as far apart in density as was convenient. Furthermore, we took care to 'bracket' the sample's density between the fluid densities (fluid 1 is less dense than the cell, and fluid 2 is more dense than the cell). In order to calculate volume and mass, the sensitivity of the SMR, relating buoyant mass to cantilever resonant frequency change, was determined with NIST size standard beads as previously reported.[2] Note that since the buoyant mass calibration factor affects all the buoyant mass terms proportionally in eqn (2), this calibration is not actually required for measuring cell density.

2.2 Materials

Buffers. Yeast was grown and measured in yeast extract plus peptone medium supplemented with 2% glucose and 1 mg ml^{-1} adenine (YEPD) and bacteria in Luria-Bertani (LB) broth (Sigma-Aldrich L2542). For the secondary fluid for the density

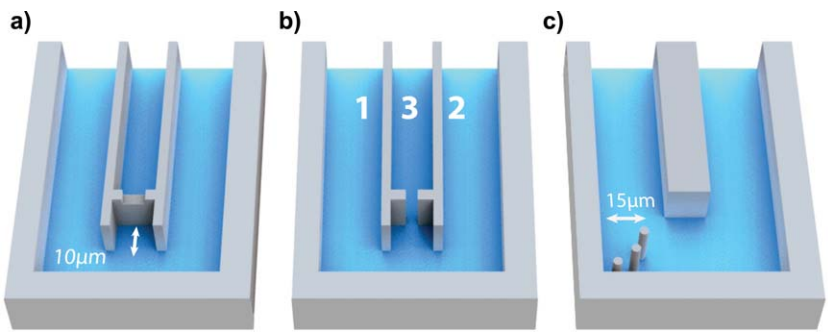

Fig. 1 Top perspective of SMRs with mechanical traps. Three-channel SMRs with different third-channel dock geometries: (**a**) 3 × 8 μm device with a 200 nm horizontal slit and (**b**) 8 × 8 μm device with a vertical 2 μm wide opening. (**c**) Columned SMR.

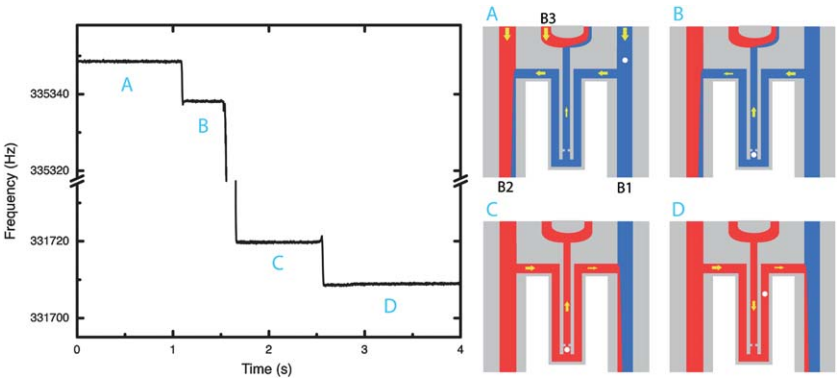

Fig. 2 SMR resonant frequency response is plotted *versus* time as the density of a 5 μm polystyrene bead is measured. **A** – SMR is filled with water. **B** – A bead is trapped. The short spike at the end of the step is due to the bead rounding the corner of the wall, before entering the pocket; **C** – Water is replaced by D_2O. **D** – The particle is ejected.

measurements we used Milli-Q ultrapure water, deuterium oxide (Sigma-Aldrich 151882) and a 1 : 9 dilution of 10x PBS (Omnipur 6505) in high-density Percoll (Sigma-Aldrich P4937, modified as reported by Grover *et al.*[4])

Cells. *Saccharomyces cerevisiae* cells (strain A2587) were grown in YEPD at 30 °C with agitation and measured about 2.5 h after the culture had been started, prior to beginning of exponential growth phase. *Escherichia coli* (ATCC 25922) were grown in LB overnight at 37 °C then diluted 1 : 100 in media 1 h before the measurement.

Polystyrene beads. The beads used in the measurements and calibrations were the size standards from Bangs Labs NT17N (1.9 μm) and Thermo Scientific 4205A (5 μm).

2.3 Results

We first applied this technique to polystyrene beads, which were measured in water ($\rho = 0.9983$ g cm^{-3}) and deuterium oxide ($\rho = 1.1046$ g cm^{-3}). All experiments were performed at 23.3 °C. The measurements, shown in Table 1 and Fig. 3 for 1.9 μm and 5 μm beads, were carried out in the 3 × 8 μm and 8 × 8 μm devices respectively. The results, $\rho_{1.9} = 1.0497 \pm 0.0010$ g cm^{-3} and $\rho_5 = 1.0491 \pm 0.0008$ g cm^{-3} (mean ± standard deviation), matched the reported density of polystyrene (~1.05 g cm^{-3}). In addition, we determined the population statistics of the calculated diameters by assuming the volume of a sphere in eqn (1). Both samples showed lower standard deviations and coefficients of variation than the ones reported by the manufacturers (Table 1).

Table 1 Density and population statistics of the diameter of polystyrene beads. Diameter was calculated from (1) assuming the volume of a sphere. Mean values (*) of diameter are the same by definition as they were used as buoyant mass calibration, therefore the values are merely indicative

			diameter um	
sample		density g cm^{-3}	measured	datasheet
1.9 μm (n = 231)	Mean	1.0497	1.9*	1.9*
	St. Dev	1 × 10^{-3}	0.03	0.03
	CV (%)	0.09%	1.4%	1.6%
5 μm (n = 247)	Mean	1.0491	5.003*	5.003*
	St. Dev	8 × 10^{-4}	0.04	0.05
	CV (%)	0.08%	0.8%	1.0%

The method was also used to measure the density of *S. cerevisiae* cells with an 8 × 8 μm SMR. The results obtained by consecutive measurements of the cells in their medium ($\rho = 1.0182$ g cm^{-3}) and PBS:Percoll ($\rho = 1.1667$ g cm^{-3}) are shown in Fig. 4. An average cell density $\rho = 1.1042 \pm 0.0057$ g cm^{-3}, CV = 0.59%, n = 244 (totaling 2 runs) was determined. This value is in accordance with single-cell yeast density measurements obtained through other methods (Table 2). The two experimental runs were measured from two samples taken from the same culture, one hour apart. The measured densities were $\rho = 1.1049 \pm 0.0068$ g cm^{-3}, CV = 0.62% for the earlier one (n = 132) and $\rho = 1.1033 \pm 0.0061$ g cm^{-3}, CV = 0.56% for the later sample (n = 112). The results for calculated mass are $m = 95.08 \pm 46.30$ pg, CV = 48.7% and volume $V = 78.1 \pm 35.3$ μm^3, CV = 45.2% and $V = 95.9 \pm 47.5$ μm^3, CV = 49.6%, respectively. The data of the two separate measurements are shown in Supplementary Fig. 1, ESI.† Volume was also measured with a Coulter Counter (Beckman Coulter, Multisizer 4), $V = 78.5 \pm 49.2$ μm^3, CV = 62.6% and $V = 91.45 \pm 58.5$ μm^3, CV = 64.0%, respectively (n = 20,000 cells).

2.4 Discussion

The results demonstrate that our method can accurately determine the density, mass, and volume of single cells to the extent that osmotic shock can be avoided or minimized and that the density of the cell being measured can be bracketed by the appropriate solution densities. More than one cell can be trapped at the same time if a cluster of cells enter simultaneously or if the flow reversal time is not short enough to prevent an additional cell from being captured. For density measurements, the capture of multiple cells will result in a measured average, which will mask the variability amongst those cells. However, these events can be detected optically or by size signatures and can be rejected by data analysis.

We further attempted to achieve the same measurement on bacterial cells (*E. coli*) with the 3 × 8 μm SMR. However, although single bacterium can be trapped within the pocket, ejection proved to be difficult without large pressure differentials due to cell adhesion to the walls. Further developments such as

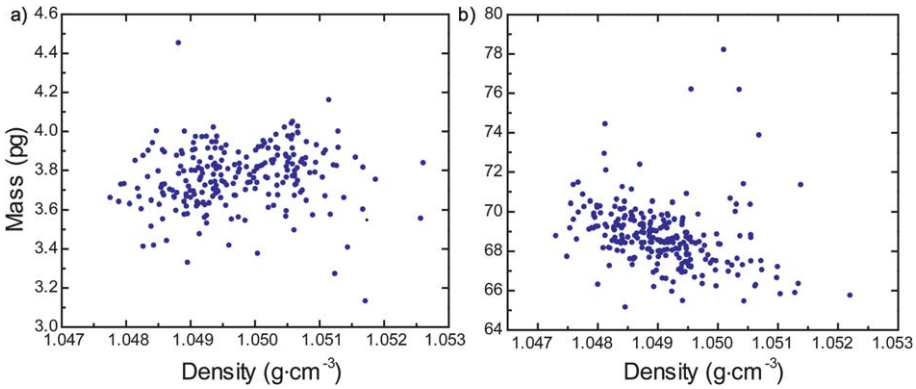

Fig. 3 Density and mass of polystyrene size standard beads measured in two different three-channel devices. Mean densities: (**a**) 1.9 μm particles $\rho = 1.0497 \pm 0.0010$ g cm^{-3}, CV = 0.09%, n = 231 (**b**) 5.003 μm particles $\rho = 1.0491 \pm 0.0008$ g cm^{-3}, CV = 0.08%, n = 247.

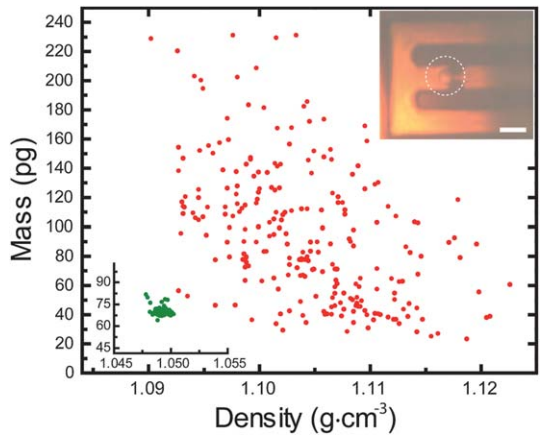

Fig. 4 Density and mass of *S. cerevisiae* cells. Mean density $\rho = 1.1042 \pm 0.0066$ g cm^{-3}, CV = 0.59%, n = 244. **Inset plot** Density and mass of 5 μm polystyrene beads measured in the same conditions as the cells. Scales are the same as the main plot. The biological variability as determined by the spread of cell measurements is less than the instrument variability as predicted by the measurement and dispersion of bead samples. **Inset picture** Immobilized cell (circled). Scale bar: 10 μm.

bacteria-resistant surfaces[16] are still required to successfully measure the density of single bacteria.

3 Columned SMRs

3.1 Method

In order to measure the drug response of single cells, we used our existing process[1] to fabricate SMRs of 15 × 20 μm cross-sectional area with 3 μm diameter trapping columns that are spaced evenly by 3 μm in a U-shape located either at the side or at the center of the cantilever apex (Fig. 1c). Two larger bypass channels (100 μm in diameter) deliver fluid to and from the SMR. Under normal device operation, a sample containing cells suspended in a carrier medium (Fig. 5, **blue**) is first loaded *via* pressure driven flow. A single cell entering the SMR that happens to be caught within the columns will result in a step-wise change in resonant frequency corresponding to an increase or decrease in total sensor mass.

Most cells flowing through the SMR follow the path of least resistance and are diverted away from the columns. In order to optimize the likelihood of trapping a cell within the columns, two additional technical components are employed. First, the pressure drop across the SMR is precisely adjusted by a combination of both ambient and hydrostatic control to reduce or eliminate fluid flow; and second, the SMR is driven at higher amplitudes to appreciate a significant centrifugal force on the cell.[17] The SMR is typically actuated only by electrostatic forces from an adjacent electrode. In order to generate sufficient vibration amplitude for guiding the cell into the columns, piezoelectric actuation tuned in phase with the electrostatic drive is superimposed. Piezoelectric actuation has been shown to produce a few microns of amplitude in SMR oscillation.[18] This in turn exerts a nanonewton-scale centrifugal force on a 10 μm polystyrene bead, which provides enough acceleration to move a bead at rest near the cantilever apex into the trapping compartment in less than a second. Although a similar approach can be used for trapping cells, cell density is less than the polystyrene density resulting in an overall smaller centrifugal force. In order to compensate for this, stop flow (or zero pressure differential) across the cantilever must be imposed

Table 2 Reported measurements of yeast density

reference	density g cm^{-3}	method
Reuß *et al.* 21	1.0952 ± 0.011	Anton Parr DMA 45 densitometer
Aiba *et al.* 22	1.090 ± 0.0112	settling velocity
Haddad *et al.* 23	1.087 ± 0.026	settling velocity
Baldwin *et al.* 24	1.1126 ± 0.010	density gradient centrifugation
Bryan al.3	1.1029 ± 0.0026	SMR + Coulter Counter
current result	1.1042 ± 0.0066	SMR

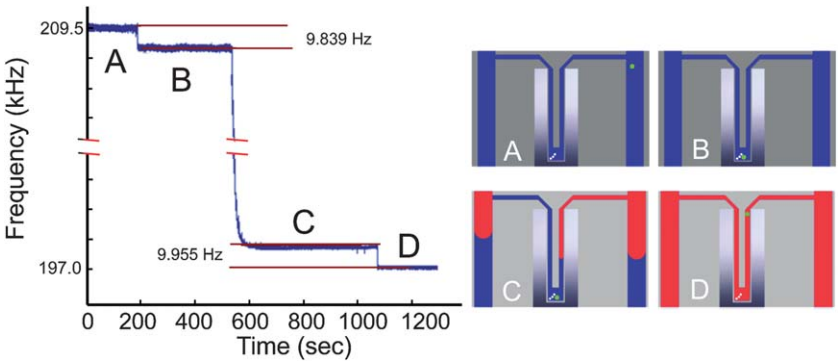

Fig. 5 Columned SMR device operation. **A** – Empty channel; **B** – 10 micron polystyrene bead (green, $\rho = 1.05$ g cm^{-2}) is trapped in H_2O (blue, $\rho = 1.00$ g cm^{-2}); **C** – Fluid is exchanged to D_2O (red, $\rho = 1.10$ g cm^{-2}); **D** – Bead is ejected from trap.

when a transiting cell arrives at the vicinity of the columns allowing the centrifugal force sufficient time to accelerate the cell into the mechanical trap. Once the cell is trapped, a pressure differential across the cantilever is resumed. This is achieved by applying pressure-driven flow to the upstream of both bypass channels. The flow rate on one side is greater than the other in order to prevent the cell from escaping the trap as a new fluid carrying a drug or stimulus enters the SMR (Fig.5, **red**). When the fluidic exchange is completed, the SMR resonant frequency stabilizes. Reversing the flow effectively removes a cell from the trap, resulting in another step-wise shift in resonant frequency.

A drug response experiment begins by employing the dynamic trapping method[2] to measure the instantaneous growth rate of the cell. The cell is then mechanically trapped within the columns as described previously, and a new fluid containing the drug is delivered as depicted in Fig. 5. Following drug delivery, the cell is ejected from the columns and dynamic flow trapping is utilized once again to monitor the buoyant mass of the cell. When compared to statically holding a cell within the SMR, monitoring buoyant mass by dynamically trapping the cell has the important advantage that the baseline signal is measured after every passage in order to correct for drift.

3.2 Materials

Buffers. Cells were grown and measured in Lebovitz's L15 medium (Invitrogen 21083027) supplemented with 10% FBS (Invitrogen no. 16000-044), 0.4% glucose (Sigma-Aldrich G8769) and 1% penicillin/streptomycin mix (Cellgro MT-30-002-CI) at 37 °C. Sodium azide (Sigma Ultra S8032-100G) was added for drug treatment experiments. Deuterium oxide (Sigma-Aldrich 151882) was used as the second fluid for the polystyrene bead measurement.

Cells. L1210 mouse lymphoblasts were grown in medium (L-15 + FBS + glucose + penstrep) inside tissue culture flasks at 37 °C and at 5% ambient carbon dioxide. Cell culture was maintained in log phase by periodically diluting and re-suspending cells in fresh medium every two days. Total cell count in culture was kept between 50×10^3 mL^{-1} and 200×10^3 mL^{-1}. To fix cells, 5 mL of a saturated culture (cell count at 1×10^6 mL^{-1}) was spun down (150 rcf for 5 min), washed with 1× PBS, and then re-suspended in 0.5 mL 100 mM phosphate buffer + 0.5 100 mM phosphate buffer solution with 7.4% Formaldehyde and 4% Glutaraldehyde. The sample was then left at room temperature overnight and later washed and re-suspended in 1× PBS. The fixed cells were kept at 37 °C overnight to ensure that any possible molecular exchange between the cells and the medium have reached equilibrium.

Polystyrene beads. The beads used in the measurements and calibrations were from Bangs Labs NT27N (10 μm).

3.3 Results

As with the three-channel SMRs, the feasibility of fluidic exchange for the columned devices was first assessed using 10 μm diameter polystyrene beads. Fig. 5 reports on this proof of concept experiment. The bead is sinking in water when it is captured in the columns. Following complete fluid replacement, it is then floating in deuterium oxide. In contrast to the three-channel SMRs, any new fluid entering the columned SMRs must first replace the contents of both bypass channels. Thus, the entire process of fluidic exchange, which typically requires 3 to 5 min, takes substantially longer than can be achieved by three-channel SMR.

We measured the growth rate of L1210 mouse lymphoblast cells before and after fluidic exchange in three conditions: 1) a single growing cell before and after a control exchange from medium to like medium; 2) a single growing cell before and after exchange from medium to medium + 1% sodium azide; 3) a single fixed cell before and after a control exchange from medium to like medium. Cells that were exchanged from medium to like medium grew at comparable rates before and after fluidic exchange (Fig. 6a), indicating that shear stress from the fluidic exchange does not alter the short-term growth properties. In contrast, cells that were exchanged from medium to medium + 1% sodium azide exhibited a negative growth rate immediately following exchange (Fig. 6b). Sodium azide causes ATP synthesis to shut down, which results in depolarization of the cell due to inhibition of active transporters on the plasma membrane in counterion exchange.[19,20] An increase in osmotic pressure inside the cell stimulates an increase in uptake of water and thereby decreases the density of the cell. As a result, the buoyant mass

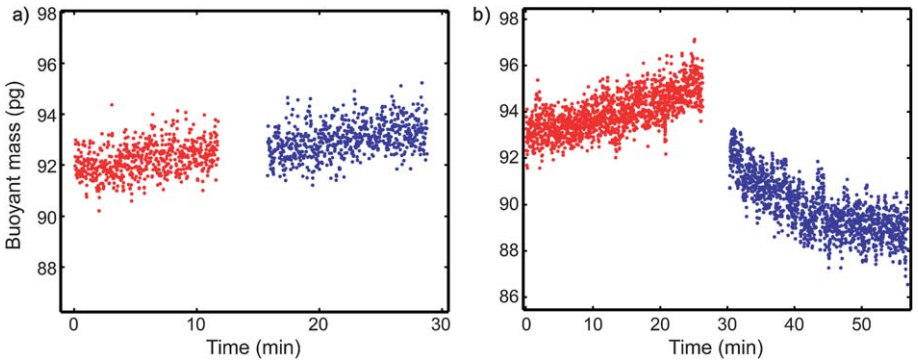

Fig. 6 The buoyant mass *versus* time of individual L1210 mouse lymphoblast cells. (**a**) Control: monitored in medium (red) and exchanged into medium (blue). (**b**) Drug delivery: monitored in medium (red) and exchanged in medium with 1% sodium azide (blue).

decreases. The negative growth rate exhibited following treatment with sodium azide is a biophysical manifestation of the cell's inability to maintain a concentration gradient across the plasma membrane. Results from additional measurements are summarized in Fig. 7.

3.4 Discussion

We demonstrated that the columned SMRs can effectively monitor the buoyant mass of a cell before and after drug treatment. However, the columned SMRs have several drawbacks: i) long-term growth studies (in excess of 60 min) have not yet been possible to achieve because shear stress from the continuous flow trapping and the fluid exchange ultimately affects cell viability, ii) small pressure fluctuations during the fluidic exchange process can cause the cell to squeeze through the column gaps and escape the trap, and iii) the entire procedure requires approximately an hour to measure the drug response from one cell. The last two drawbacks, when taken together, resulted in an effective throughput of about one cell per day. Nevertheless, the method in its current state can be used to gain biophysical insight into how drugs alter the ability of a cell to uptake nutrients immediately following exposure to a drug.

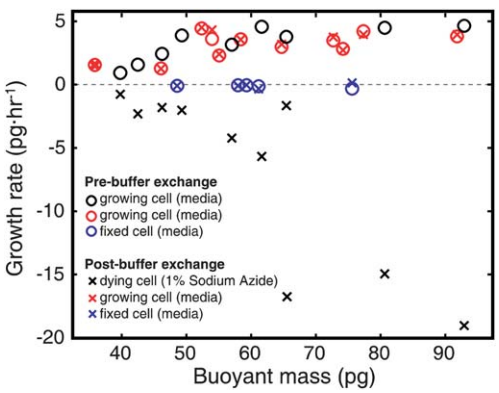

Fig. 7 The growth rates of all L1210 mouse lymphoblast cells monitored before and after fluidic exchange. The fixed cell measurements determined the noise floor of the technique to be -0.1296 ± 0.1109 pg·hr^{-1} before the exchange and -0.0809 ± 0.1697 pg·hr^{-1} after the exchange.

Conclusion

Our work augments current SMR capabilities with single-cell manipulation techniques based on mechanical trapping structures. This capability enables measurements that are not possible using flow-through mass sensing. The ability to measure the buoyant mass of an individual cell in two fluids allows its density as well as its response to a drug to be measured. We measured the density, mass, and volume of individual yeast cells in their culture medium and in PBS:Percoll solution. We also measured the dynamics of buoyant mass accumulation and loss in mouse lymphoblast cells before and after complete buffer replacement with and without the presence of a drug or stimulus.

We developed two approaches for making these measurements. In the first, three-channel SMRs capture single cells and rapidly exchange the surrounding buffer for a new fluid. Consecutive buoyant mass measurements in different fluids are rapidly acquired without the need for microfluidic mixing. This approach is not optimal for monitoring growth behavior of the cells prior to and after drug delivery as the presence of a third channel introduces fluidic pressure variations that prevent stable dynamic flow trapping. To address this limitation, we developed columned SMRs that enable a complete fluid exchange throughout the system by temporarily capturing a cell. Dynamic flow trapping can be resumed without hindrance following fluid exchange, thereby allowing for effective growth monitoring before and after drug delivery.

Acknowledgements

This work was supported by the Institute of Collaborative Biotechnologies through contract no. W911NF-09-D-0001 from the US Army Research Office and the National Cancer Institute contracts R21 CA137695 and Physical Sciences Oncology Center U54CA143874. The authors would like to thank the Kirschner lab at Harvard Medical School for providing L1210 Mouse Lymphoblast cells as well as the Amon lab at the Massachusetts Institute of Technology for providing *S. cerevisiae* cells (strain A2587). The authors would also like to thank William Grover for his invaluable comments and help with the manuscript. Y.W. acknowledges support through an NSF graduate fellowship. F. F.D. acknowledges support from Fundação para a Ciência e a Tecnologia, Portugal, through a graduate fellowship (SFRH/

BD/47736/2008). S.S. acknowledges support from KEF, South Korea, through a graduate fellowship. T.P.B. acknowledges support by the Max Planck Society and the Max Planck Institute for Biophysical Chemistry.

References

1 T. P. Burg, M. Godin, S. M. Knudsen, W. Shen, G. Carlson, J. S. Foster, K. Babcock and S. R. Manalis, *Nature*, 2007, **446**, 1066–1069.
2 M. Godin, F. F. Delgado, S. Son, W. H. Grover, A. K. Bryan, A. Tzur, P. Jorgensen, K. Payer, A. D. Grossman, M. W. Kirschner and S. R. Manalis, *Nat. Methods*, 2010, **7**, 387–390.
3 A. K. Bryan, A. Goranov, A. Amon and S. R. Manalis, *Proc. Natl. Acad. Sci. U. S. A.*, 2010, **107**, 999–1004.
4 W. H. Grover, A. K. Bryan, M. Diez-Silva, S. Suresh, J. M. Higgins and S. R. Manalis, *Proc Natl Acad Sci U S A*, 2011.
5 M. Evander, L. Johansson, T. Lilliehorn, J. Piskur, M. Lindvall, S. Johansson, M. Almqvist, T. Laurell and J. Nilsson, *Anal. Chem.*, 2007, **79**, 2984–2991.
6 D. S. Gray, J. L. Tan, J. Voldman and C. S. Chen, *Biosens. Bioelectron.*, 2004, **19**, 771–780.
7 D. Issadore, T. Franke, K. A. Brown, T. P. Hunt and R. M. Westervelt, *J. Microelectromech. Syst.*, 2009, **18**, 1220–1225.
8 R. M. Johann, *Anal. Bioanal. Chem.*, 2006, **385**, 408–412.
9 M. Ozkan, M. Wang, C. Ozkan, R. Flynn, A. Birkbeck and S. Esener, *Biomed. Microdevices*, 2003, **5**, 61–67.
10 A. Valero, F. Merino, F. Wolbers, R. Luttge, I. Vermes, H. Andersson and A. van den Berg, *Lab Chip*, 2005, **5**, 49–55.
11 A. A. Werdich, E. A. Lima, B. Ivanov, I. Ges, M. E. Anderson, J. P. Wikswo and F. J. Baudenbacher, *Lab Chip*, 2004, **4**, 357–362.
12 D. Di Carlo, N. Aghdam and L. P. Lee, *Anal. Chem.*, 2006, **78**, 4925–4930.
13 D. Di Carlo, L. Y. Wu and L. P. Lee, *Lab Chip*, 2006, **6**, 1445–1449.
14 M. C. Kim, Z. H. Wang, R. H. W. Lam and T. Thorsen, *Journal of Applied Physics*, 2008, 103.
15 A. R. Wheeler, W. R. Throndset, R. J. Whelan, A. M. Leach, R. N. Zare, Y. H. Liao, K. Farrell, I. D. Manger and A. Daridon, *Anal. Chem.*, 2003, **75**, 3581–3586.
16 G. Cheng, G. Z. Li, H. Xue, S. F. Chen, J. D. Bryers and S. Y. Jiang, *Biomaterials*, 2009, **30**, 5234–5240.
17 J. Lee, W. Shen, K. Payer, T. P. Burg and S. R. Manalis, *Nano Lett.*, 2010, **10**, 2537–2542.
18 J. Lee, R. Chunara, W. Shen, K. Payer, K. Babcock, T. P. Burg and S. R. Manalis, *Lab Chip*, 2011, **11**, 645–651.
19 J. M. Davies, C. Brownlee and D. H. Jennings, *J. Exp. Bot.*, 1990, **41**, 449–456.
20 J. C. Riemersma, *Biochim. Biophys. Acta, Bioenerg.*, 1968, **153**, 80–87.
21 M. Reuss, D. Josic, M. Popovic and W. K. Bronn, *Eur. J. Appl. Microbiol. Biotechnol.*, 1979, **8**, 167–175.
22 S. Aiba, S. Kitai and H. Heima, *J. Gen. Appl. Microbiol.*, 1964, **10**, 243.
23 S. A. Haddad and C. C. Lindegren, *Applied Microbiology*, 1953, **1**, 153–156.
24 W. W. Baldwin and H. E. Kubitschek, *J Bacteriol*, 1984, **158**, 701–704.

